Contrib Mineral Petrol (2003) 146: 356–369
DOI 10.1007/s00410-003-0503-9

ORIGINAL PAPER

Carrie R. Brugger · A. Dana Johnston
Katharine V. Cashman

Phase relations in silicic systems at one-atmosphere pressure

Received: 4 September 2002 / Accepted: 27 May 2003 / Published online: 9 October 2003

Abstract An important control on magma rheology is the extent to which the magma crystallizes during ascent as a result of the effective undercooling created by volatile exsolution. To assess this undercooling, we need to know the final (anhydrous) one-atmosphere phase relations of silicic magmas. For this reason, we have performed one-atmosphere controlled-fO_2 crystallization experiments on dacitic to rhyolitic melt compositions (67–78 wt% SiO_2) and determined equilibrium phase assemblages, melt fractions, and some phase compositions over a range of temperatures. Experiments were run at oxygen fugacities between NNO + 1 and NNO + 2 and temperatures of 1,000 to 1,250°C. Constant phase compositions and sample crystallinities in runs longer than 3.5 days suggest that these runs closely approached compositional equilibrium. Additionally, melting experiments with similar compositions yielded results closely resembling those obtained in crystallization experiments. All samples have liquidus temperatures between 1,250 and 1,200 °C, with plagioclase the liquidus phase for the two most mafic samples and quartz for the most silicic sample. When associated glass compositions are projected into the Qz-Ab-Or system they define a revised one-atmosphere quartz-feldspar cotectic 5–10% less quartz normative than previously estimated. Glass compositions from each sample plot along this cotectic between 1,100 and 1,000 °C, consistent with the plagioclase-quartz co-crystallization textures found in runs at these temperatures. This cotectic constrains glass compositions to a maximum silica content of 76 ± 1 wt% SiO_2. Reported glass compositions in excess of 77 wt% SiO_2 in volcanic samples suggest non-equilibrium crystallization, perhaps a consequence of large melt undercoolings.

Editorial responsibility: I. Carmichael

C. R. Brugger (✉) · A. D. Johnston · K. V. Cashman
Department of Geological Sciences, 1272 University of Oregon, Eugene, OR 97403–1272, USA
E-mail: cbrugger@geology.cwu.edu
Tel.: +1-509-9631628
Fax: +1-509-9632821

Present address: C. R. Brugger
Department of Geological Sciences,
Central Washington University,
400 E 8th Ave, Ellensburg, 98926-7418 WA, USA

Introduction and previous investigations

As hydrous magmas decompress during ascent, they undergo phase changes (vesiculation and/or crystallization) that alter their physical properties, which in turn affect continued ascent and eruption. Feedback mechanisms created by these processes have been used to explain transitions in eruptive behavior from explosive to effusive and the cyclicity in eruptive behavior observed during recent eruptions of andesitic volcanoes (e.g., Sparks 1997; Voight et al. 1999; Melnik and Sparks 1999). However, processes occurring at shallow levels in volcanic conduits and domes are poorly constrained because of the absence of experimental data on one-atmosphere phase relations in natural intermediate and silicic melts. The lack of one-atmosphere data stands in contrast to the extensive experimental work that has been completed in simple granitic systems involving quartz and feldspar (e.g., An-Ab, Qz-Ab-Or, Qz-An-Ab, etc.) at higher pressures (see Johannes and Holtz (1996) for a summary).

Phase relations in the haplogranite system Qz-Ab-Or in the pressure range of 50–3,500 MPa have been well constrained for water-saturated conditions (Tuttle and Bowen 1958; Luth et al. 1964; Merrill et al. 1970; Steiner 1970; Huang and Wyllie 1975; Steiner et al. 1975), for water-undersaturated conditions (Ebadi and Johannes 1991; Holtz et al. 1992a), and for dry compositions (Huang and Wyllie 1975; Ebadi and Johannes 1991). Haplogranite subsystems such as Qz-Ab and Qz-Or, with and without water, have also been studied extensively to determine liquidus and solidus phase relations and eutectic liquid compositions at pressures of 100–1,000 MPa (Schairer and Bowen 1955, 1956; Tuttle and

Bowen 1958; Shaw 1963; Luth et al. 1964; Luth 1969; Lambert et al. 1969; Bohlen et al. 1983; Boettcher et al. 1984; Pichavant et al. 1992; Holtz et al. 1992a).

Experimental studies in related systems are not as well covered as in the haplogranite system. The effects of excess alumina (peraluminous haplogranite system; Qz-Ab-Or-Al_2O_3) have been examined at 200 MPa in H_2O-saturated and undersaturated experiments (Dimitriadis 1978; Voigt and Burnham 1983; Holtz et al. 1992b; Joyce and Voigt 1994). Addition of alumina decreases the cotectic temperature and shifts the quartz-feldspar cotectic towards more quartz-rich compositions. Phase relations in the tonalite system Qz-Ab-An-H_2O have been investigated via melting experiments at 500 and 200 MPa (Yoder 1968; Johannes 1978, 1989; Bartels 1987). Within this system (and others), reaction rates are strongly dependent on temperature. Equilibrium can apparently be reached at 1,000 °C after only 1 h, but requires experiments in excess of 10 days below 790 °C (Johannes 1978). Time series studies suggest that experiments in the Qz-Ab-An-H_2O system at 730 °C would need to run an estimated 100,000 years to reach equilibrium (Johannes 1978). Johannes et al. (1994) found that addition of excess Al_2O_3 to the tonalite system produces faster reaction rates and shifts the quartz-feldspar cotectic towards the Qz-apex. Additional studies at pressures of 100–800 MPa have extended the haplogranite system to include anorthite (An; James and Hamilton 1969; Winkler and Ghose 1973; Whitney 1975; Winkler et al. 1975, 1977; Johannes 1984). Kinetic studies in the granite system Qz-Ab-Or-An-H_2O have found that approach to equilibrium is extremely sluggish below 800 °C, but above this temperature equilibrium compositions can be reached in runs of only a few days (Johannes and Holtz 1996). Whitney (1975) found that slightly increasing the An-content increases the liquidus temperature about 150 °C above that determined by Tuttle and Bowen (1958) for the haplogranite (Qz-Ab-Or) system. Addition of An also increases the solidus temperature, however the effect is very small (e.g., 10 °C when albite is replaced by plagioclase An_{40}; Johannes 1984). As noted by Johannes and Holtz (1996), the presence of phases in addition to plagioclase and quartz may be even more important in affecting the compositions of melts, their temperatures of formation, and the rates at which equilibrium is attained.

While there are abundant data on feldspars and quartz in simple two-, three-, four-, and five-component systems, fewer phase equilibria studies have been performed in multi-component Fe- and Mg-bearing silicic systems (Clemens and Wall 1981; Huang and Wyllie 1981; Naney 1983; Rutherford et al. 1985; Clemens et al. 1986; Conrad et al. 1988; Le Breton and Thompson 1988; Puziewicz and Johannes 1988; Rutherford and Devine 1988; Vielzeuf and Holloway 1988; Johnson and Rutherford 1989; Holtz and Johannes 1991; Scaillet et al. 1995), and none of these were conducted at one-atmosphere. Previous work in silicic systems at one-atmosphere appears to be limited to the plagioclase melting loop in the system Ab-An (Bowen 1913; Tsuchiyama and Takahashi 1983; Muncill and Lasaga 1987; Johannes et al. 1994) and the Qz-Ab-Or system (Schairer and Bowen 1935; Schairer 1950). In some of their earliest experiments Schairer and Bowen (e.g., 1935) could not locate the one-atmosphere equilibrium liquidus in the Qz-Ab-Or system because their highly polymerized dry melts would not nucleate crystals, even in runs as long as 5 years. Their efforts (e.g., Schairer and Bowen 1935; Schairer 1950) are often cited by other researchers as evidence that anhydrous quartz-feldspar systems are too viscous to reach equilibrium at one-atmosphere (e.g., Cashman 1992; Holtz et al. 2001). Therefore, experiments in such systems at pressures below ~50 MPa do not appear in the literature. However, to our knowledge, no one has ever conducted one-atmosphere experiments in dry silicic systems that contain natural levels of network modifiers such as Fe and Mg. Our results suggest that the presence of these network modifiers reduces the viscosity and increases reaction rates enough to allow experiments to reach equilibrium on experimental time scales (e.g., Johannes et al. 1994). So while we cannot directly examine one-atmosphere phase relations in the haplogranite system, we can study them in analogous natural multi-component systems, which also provide better descriptions of natural silicic magmas.

Using the phase assemblages, abundances, and compositions produced in one-atmosphere experiments one may evaluate the extent to which volcanic samples achieve equilibrium at near-surface conditions. This in turn can provide constraints on the crystallization behavior of a particular magma. Some magmas may crystallize steadily as they ascend and decompress, as appears common with basalts and basaltic andesites (e.g., Hammer et al. 2000; Gardner et al. 1998). Others may continuously degas as they rise, overstep their liquidus, and then, after some lag time, crystallize near or at the surface (e.g., Hammer et al. 1999; Cashman and Blundy 2000). In the former case, crystals would continuously re-equilibrate with the melt as the magma rose, sometimes leading to zoned phenocrysts with high pressure compositions in their interiors and low pressure compositions at their margins. In the other instance, the melt would experience large effective undercooling (due to decompression) and respond by crystallizing low pressure, near-surface phase assemblages and compositions late in the ascent process. Knowledge of one-atmosphere phase relations and compositions may therefore help us examine syn-eruptive crystallization and its effects on volcanic eruptions. In this study, we conduct one-atmosphere, controlled fO_2, crystallization experiments on select compositions to determine their equilibrium phase assemblages and compositions over a range of temperatures. A smaller number of melting experiments, constituting quasi-reversals, provide confirmation of the crystallization runs.

The results reported here include the identities of the stable phases and, when possible, phase compositions for given composition-temperature conditions, and

provide a basis for determining whether natural samples achieved near-surface equilibrium prior to quenching. These comparisons can be used to examine the driving forces of volcanic eruptions when magma intrudes to shallow levels, and to better understand the kinetics of degassing-induced crystallization.

Methods

Starting materials

As starting material we used individual pyroclasts produced during the 1986 eruption of Augustine Volcano, Alaska. The samples encompass a large range in bulk composition, from basaltic andesite to dacite, and groundmass (glass plus microlites) compositions from dacite to rhyolite. Two different types of starting materials were employed: (1) synthetic glasses (samples 816-3, 722-5, and 816-4 of Table 1) prepared to simulate the natural groundmass compositions, and hereafter referred to as "initial melt" compositions, and (2) natural samples (A and B of Table 1) prepared by crushing Augustine pyroclasts and removing large crystals.

Previous kinetic investigations have shown that equilibrium is best approached in crystallization experiments when crushed glasses are used as starting materials and they are brought directly to the run temperature (Becker et al. 1998), a method that we employed. Melting experiments were run on two natural samples. One of these (A) had a composition quite similar to one of the synthetic samples (816-3) (see Table 1) and as such provided the opportunity to evaluate whether the crystallization experiments and melting experiments produced similar results. The other (B) had a composition quite different from the synthetics, but nonetheless was useful in constructing a summary phase diagram presented in the discussion section.

Initial melt compositions were estimated by analysis of the groundmass using a broad beam (30 μm) on a Cameca SX-50 electron probe microanalyzer (EPMA) at the University of Oregon, operating at 15 kV acceleration voltage and 5 nA beam current. Care was taken to avoid crystals larger than ~50 μm across due to their zoning, resorption, and sieve textures. Data reduction used a PAP correction model (Pouchou and Pichoir 1991). Depending on the homogeneity of the sample, 26–57 points were analyzed and averaged to determine the average groundmass melt composition (Table 1). The three synthetic compositions were created by combining appropriate proportions of oxide (Mg, Al, Si, Ti, Fe^{3+}) and carbonate (Na, K, Ca) powders, decarbonating them in a controlled atmosphere that reduced much of the Fe_2O_3 to FeO, and then fusing them.

Natural rock starting materials were created by lightly crushing selected samples from Augustine Volcano and removing all crystals ≥200 μm in diameter. Once the largest crystals were removed, the remaining groundmass was hand ground in an agate mortar for approximately 30 minutes. Consequently, the starting material for the melting experiments consisted of shards of glass and small crystals of plagioclase, pyroxene, and iron-titanium oxides (Fe-Ti oxides).

Table 1 Bulk compositions of synthetic initial melts (wt%)

Sample	SiO_2	TiO_2	Al_2O_3	FeO*	MgO	CaO	Na_2O	K_2O
816-3	67.19	0.50	16.45	3.48	1.89	5.10	4.29	1.11
722-5	73.71	0.87	14.04	2.30	0.54	2.81	4.09	1.65
816-4	78.07	0.38	12.84	1.64	0.26	1.21	3.86	1.75
Natural A	67.41	0.36	17.37	2.27	1.08	5.56	4.15	1.81
Natural B	61.16	0.60	16.38	5.30	3.19	6.84	5.10	1.44

FeO* indicates that all iron is recalculated as ferrous iron

Experimental procedures

All experiments were conducted at one atmosphere in Deltech gas-mixing vertical quench furnaces with temperature monitored by Pt-$Pt_{90}Rh_{10}$ thermocouples calibrated against the melting point of gold. Oxygen fugacity was held between the NNO + 1 (one log unit more oxidizing than the $Ni + 1/2O_2 = NiO$ buffer; Huebner and Sato 1970) and NNO + 2 buffers using CO_2/H_2 gas mixtures and monitored using Y-doped ZrO_2 solid electrolyte oxygen sensors. Sample powders were suspended from 0.005-inch diameter Pt wire loops at the run temperature for 77–413 h and then quenched in water. No special effort was made to prevent iron loss to the platinum wire, as these samples contained very little iron and the mass of platinum in contact with the samples was negligible. Similarly, no special procedures were employed to minimize potential Na-volatilization during the experiments themselves. However, the same is true of the super-solidus experiments that were analyzed to determine the bulk compositions of the samples. Each synthetic sample was run over a range of temperatures from its liquidus to 1,000 °C. The run conditions and resulting assemblages are tabulated in Table 2.

Analytical methods

Textures and phase compositions were collected using a JEOL JSM-6300XV scanning electron microscope (SEM) and Cameca SX-50 EPMA at the University of Oregon. To minimize sodium loss while analyzing glass with the EPMA, a 5-nA beam current and a 20-μm diameter spot size were used with an accelerating voltage of 15 kV (e.g., Morgan and London 1996). Where crystallinity was relatively high and large glass patches could not be found, spot sizes of 10 μm or 3 μm were used. As smaller spot sizes lead to loss of Na during analyses, a sodium loss correction factor, based on the linear depletion of sodium counts with time under these conditions, was applied to the 10 and 3 μm analyses (Nielsen and Sigurdsson 1981; Roman 2001, Appendix D). These corrections were typically on the order of 0.01–0.12 wt%. Crys-

Table 2 Summary of run conditions and products

Sample	Run no.	T (°C)	log fO_2	Duration (days)	Phases present[a]	Crystals[b] (%)
816-3	13	1,250	−5.01	7.7	gl	0.0
	12	1,190	−5.56	7.7	gl, pl	5.1
	11	1,150	−6.16	8.0	gl, pl	17.2
	7	1,100	−7.80	3.8	gl, pl, ox, opx, qtz	40.6
	15	1,050	−7.48	9.0	gl, pl, ox, opx, qtz, cpx	55.4
	17	1,000	−8.22	10.0	gl, pl, ox, opx, qtz, cpx	70.0
722-5	25	1,250	−5.01	7.1	gl	0.0
	23	1,200	−5.56	7.1	gl, pl	−5.1
	21	1,150	−6.16	8.9	gl, pl, qtz	1.2
	22	1,090	−6.80	7.1	gl, pl, qtz, ox	12.7
	20	1,040	−7.48	8.9	gl, pl, qtz, ox	35.5
	24	990	−8.22	10.2	gl, pl, qtz, ox, opx	54.9
816-4	8	1,225	−6.28	7.0	gl	0.0
	5	1,200	−6.56	3.2	gl, qtz	1.1
	14	1,140	−7.16	9.0	gl, qtz, pl, ox	1.7
	2	1,100	−7.80	3.2	gl, qtz, pl, ox	15.5
	3	1,050	−8.48	3.4	gl, qtz, pl, ox	30.0
	6	1,050	−8.48	8.6	gl, qtz, pl, ox	32.2
	10	1,050	−8.48	17.2	gl, qtz, pl, ox	33.7
	16	990	−9.22	10.0	gl, qtz, pl, ox	44.8
Natural A	35[c]	~1,400	-	3.0	gl	
	31	1,140	−7.16	7.3	gl, pl	
	33	1,090	−7.80	8.0	gl, pl, qtz, ox, opx	
	29	1,040	−8.48	7.3	gl, pl, qtz, ox, opx, cpx	
Natural B	26[c]	~1,400	-	2.0	gl	
	27	1,190	−5.56	7.8	gl, pl	
	30	1,150	−6.16	7.3	gl, pl	
	34	1,100	−6.80	8.0	gl, pl, ox, opx	
	28	1,050	−7.48	7.8	gl, pl, ox, opx, cpx	

[a] *gl* Glass, *pl* plagioclase, *qtz* silica phase, *ox* oxides, *opx* orthopyroxene, *cpx* clinopyroxene; phases listed in order of appearance

[b] Calculated assuming K_2O is completely incompatible; see text

[c] Temperature and oxygen fugacity were not monitored in these experiments as the goal was to completely melt the samples and determine their bulk composition

talline phases were analyzed using a focused (1 μm) beam. All analyses were assumed to be anhydrous and were therefore normalized to 100% after the Na correction, when applied. Original totals ranged from 97 to 103%. For each phase, 8 to 15 points were analyzed and then averaged. Individual glass analyses that contained statistical outliers (values 0.1 wt% greater than or less than 2σ standard deviations from the mean) for one or more elements were discarded and the average compositions were recalculated. A list of average glass compositions for each run is given in Table 3; a complete list of original analyses can be found in Brugger (2001). We are confident of our glass data but found the crystalline phases extremely difficult to analyze due to their small sizes; every crystal analysis contained glass contamination at some level. We were able to correct for this reasonably well with the plagioclase analyses (as described below) and thus report these (corrected) data here. The same cannot be said of the pyroxenes and oxides so no analyses of these phases are reported.

Mineral formulas were calculated for all plagioclase analyses (Table 4). The highest temperature runs gave the most stoichiometrically accurate cation totals because lower temperature runs contained very small (<1 μm in diameter) crystals that were difficult to analyze without contamination from adjacent glass. We used the MgO and TiO_2 contents of our plagioclase analyses to assess the extent of glass contamination. An appropriate amount of glass contaminant was then subtracted from each analysis to make the Ti and/or Mg content zero. The plagioclase analyses with the best stoichiometries were then averaged (Table 4). As noted above, this correction could not be applied to the pyroxene data, as Ti and Mg are present in these minerals. However, the data were adequate to identify the phases as pyroxenes and to distinguish between clinopyroxene and orthopyroxene.

The crystallinity of each run (Table 2) was calculated using K_2O abundances and the batch melting equation, assuming perfect incompatibility of potassium in all crystallizing phases. However, as a small amount of K_2O (up to 0.4 wt%) are present in the plagioclase crystals (Table 4), calculated crystallinities should be regarded as a minima. If the error associated with analyzing potassium is considered, calculated crystallinity errors on the order of 5–6% (absolute) are reasonable.

Results

Approach to equilibrium

The time necessary to reach equilibrium was assessed by comparing experiments of different durations to determine how long they needed to run before the phase assemblages and compositions stabilized. The most silicic sample, 816-4, was run at 1,050 °C for 3.5, 8.6, and 17.2 days, and all of these runs produced the same glass composition within error (Fig. 1). Similarly the total crystallinity in these runs, calculated from K_2O concentrations, was constant at 32 ± 2 wt% (Fig. 2). On the basis of these results, we conclude that runs of 3.5 days or longer acceptably approached equilibrium at 1,050 °C with our most silicic sample, 816-4. As higher temperatures or less silicic compositions would lead to acceptable results in shorter duration runs, we have also retained the data from runs of 3.2 days with sample 816-4 at 1,100 and 1,200 °C. Melting experiments run in parallel with crystallization experiments produced very similar results, supporting our contention that these runs closely approached equilibrium.

Table 3 Electron microprobe analyses of glasses

	Run no.	*n*	SiO_2	TiO2	Al_2O_3	FeO*	MgO	CaO	Na_2O	K_2O
816-3	13	10	67.2 (3)	0.50 (18)	16.5 (1)	3.48 (34)	1.89 (6)	5.09 (12)	4.29 (9)	1.11 (7)
	12	10	67.8 (5)	0.48 (18)	15.8 (2)	3.45 (34)	1.91 (11)	4.68 (16)	4.72 (17)	1.17 (6)
	11	10	69.6 (2)	0.64 (15)	14.3 (3)	4.11 (29)	2.25 (10)	3.92 (13)	3.85 (20)	1.34 (6)
	7	10	76.4 (7)	0.74 (12)	12.4 (4)	3.30 (21)	1.10 (7)	2.67 (22)	1.55 (25)	1.87 (6)
	15	9	76.9 (5)	0.65 (19)	11.9 (4)	2.39 (19)	0.73 (5)	1.92 (31)	2.93 (14)	2.49 (10)
	17	9	76.4 (9)	0.68 (32)	12.5 (7)	1.83 (18)	0.42 (7)	1.32 (40)	3.08 (23)	3.70 (26)
722-5	25	5	73.7 (4)	0.87 (6)	14.0 (1)	2.30 (23)	0.54 (2)	2.81 (18)	4.09 (9)	1.65 (7)
	23	7	73.7 (3)	0.91 (12)	14.0 (2)	2.39 (12)	0.58 (4)	2.86 (4)	4.00 (8)	1.57 (9)
	21	6	75.4 (7)	0.95 (15)	12.9 (3)	2.43 (23)	0.61 (5)	2.23 (7)	3.80 (19)	1.67 (5)
	22	10	76.7 (4)	0.86 (24)	12.3 (1)	2.24 (19)	0.71 (4)	1.50 (16)	3.78 (25)	1.89 (10)
	20	10	76.5 (6)	0.68 (18)	12.3 (4)	1.93 (13)	0.88 (7)	1.06 (10)	4.04 (17)	2.56 (10)
	24	8	76.4 (5)	0.65 (22)	12.7 (5)	1.33 (11)	0.53 (6)	0.64 (12)	4.13 (18)	3.66 (24)
816-4	8	10	78.1 (5)	0.38 (9)	12.8 (3)	1.64 (20)	0.26 (5)	1.21 (14)	3.86 (17)	1.75 (11)
	5	11	77.5 (7)	0.33 (9)	13.2 (3)	1.75 (26)	0.42 (5)	1.93 (13)	3.10 (31)	1.77 (9)
	14	9	77.6 (2)	0.38 (7)	12.8 (2)	1.69 (14)	0.40 (5)	1.57 (12)	3.80 (16)	1.78 (4)
	2	11	76.8 (6)	0.42 (21)	13.2 (3)	2.05 (16)	0.53 (7)	1.17 (11)	3.78 (15)	2.07 (10)
	3	11	76.5 (4)	0.42 (8)	13.2 (3)	2.14 (17)	0.58 (6)	0.80 (7)	3.83 (16)	2.50 (16)
	6	13	77.1 (7)	0.26 (7)	13.3 (4)	1.55 (22)	0.63 (8)	0.79 (9)	3.71 (25)	2.58 (17)
	10	14	77.0 (3)	0.34 (14)	13.3 (1)	1.72 (20)	0.59 (3)	0.61 (6)	3.82 (25)	2.64 (8)
	16	12	75.7 (9)	0.32 (18)	13.5 (5)	2.46 (29)	0.67 (8)	0.46 (4)	3.73 (19)	3.17 (12)
Natural A	35	6	67.4 (4)	0.36 (6)	17.4 (2)	2.27 (13)	1.08 (4)	5.56 (15)	4.15 (13)	1.81 (6)
	31	9	72.0 (3)	0.38 (7)	14.0 (2)	2.56 (18)	1.34 (9)	3.55 (14)	4.36 (8)	1.80 (11)
	33	9	74.2 (3)	0.38 (14)	12.7 (2)	2.92 (13)	1.23 (8)	2.77 (15)	3.85 (13)	1.92 (19)
	29	9	76.9 (6)	0.49 (14)	12.1 (1)	2.54 (18)	0.60 (7)	1.61 (16)	3.22 (49)	2.50 (8)
Natural B	26	8	61.2 (4)	0.60 (8)	16.4 (2)	5.30 (24)	3.19 (7)	6.84 (15)	5.10 (11)	1.43 (4)
	27	10	62.4 (4)	0.67 (12)	16.2 (2)	5.28 (34)	3.43 (9)	6.42 (15)	4.51 (9)	1.15 (13)
	30	10	63.8 (7)	0.79 (14)	14.9 (2)	5.88 (34)	3.84 (23)	5.82 (22)	3.81 (18)	1.20 (11)
	34	10	67.9 (5)	0.99 (14)	13.1 (2)	5.84 (37)	2.08 (14)	4.76 (15)	3.76 (13)	1.61 (10)
	28	11	76.1 (7)	0.95 (25)	11.9 (4)	2.87 (21)	0.88 (15)	2.25 (29)	2.53 (18)	2.47 (13)

n number of analyses
Figures in parentheses represent one standard deviation of replicate analyses in terms of least units cited. Thus, 1.89 (6) should be read 1.89 ± 0.06 and 4.72 (17) is 4.72 ± 0.17
FeO* indicates that all iron is recalculated as ferrous iron

Table 4 Electron microprobe analyses and structural formulae of plagioclase

	Run no.	*n*	SiO_2	TiO_2	Al_2O_3	FeO*	MgO	CaO	Na_2O	K_2O	Cations (based on 8 oxygens)								An-Ab-Or proportions		
											Si	Ti	Al	Fe	Mg	Ca	Na	K	An	Ab	Or
816-3	12	9	51.64[a,b]	0.01	30.40	0.65	0.03	13.27	3.98	0.03	2.35	0.00	1.63	0.02	0.00	0.65	0.35	0.00	0.65	0.35	0.00
	11	10	51.48	0.03	29.85	1.13	0.05	13.61	3.84	0.02	2.35	0.00	1.61	0.04	0.00	0.67	0.34	0.00	0.66	0.34	0.00
	7	8	53.61	0.13	28.27	0.84	0.01	12.43	4.59	0.11	2.44	0.00	1.52	0.03	0.00	0.61	0.40	0.01	0.60	0.40	0.01
	15	7	53.11	0.04	28.08	1.43	0.27	11.85	5.18	0.03	2.42	0.00	1.51	0.05	0.02	0.58	0.46	0.00	0.56	0.44	0.00
	17	6	57.71	0.06	25.64	1.02	0.23	8.75	6.57	0.02	2.60	0.00	1.36	0.04	0.02	0.42	0.57	0.00	0.42	0.58	0.00
722-5	21	8	52.64	0.04	29.10	0.91	0.01	12.99	4.24	0.08	2.40	0.00	1.56	0.03	0.00	0.63	0.37	0.00	0.63	0.37	0.00
	22	7	54.78	0.12	27.88	0.62	0.00	11.55	5.02	0.02	2.48	0.00	1.49	0.02	0.00	0.56	0.44	0.00	0.56	0.44	0.00
	20	6	58.95	0.19	25.09	0.63	0.04	8.52	6.43	0.15	2.64	0.01	1.32	0.02	0.00	0.41	0.56	0.01	0.42	0.57	0.01
	24	6	62.82	0.45	22.65	0.98	0.00	6.53	6.35	0.21	2.78	0.02	1.18	0.04	0.00	0.31	0.55	0.01	0.36	0.63	0.01
816-4	14	10	44.17	0.08	37.77	0.84	0.00	13.60	3.53	0.02	2.03	0.00	2.05	0.03	0.00	0.67	0.31	0.00	0.68	0.32	0.00
	2	7	56.34	0.06	27.75	0.32	0.00	10.83	4.57	0.13	2.53	0.00	1.47	0.01	0.00	0.52	0.40	0.01	0.56	0.43	0.01
	6	7	61.70	0.26	23.27	0.72	0.00	8.27	5.62	0.17	2.74	0.01	1.22	0.03	0.00	0.39	0.48	0.01	0.44	0.55	0.01
	16	8	63.39	0.21	23.50	0.22	0.00	6.31	5.94	0.43	2.79	0.01	1.22	0.01	0.00	0.30	0.51	0.02	0.36	0.61	0.03
Natural A	31	4	51.92	0.00	29.84	1.04	0.25	13.25	3.54	0.16	2.37	0.00	1.60	0.04	0.02	0.65	0.31	0.01	0.67	0.32	0.01
	33	7	53.74	0.05	28.84	0.72	0.08	12.18	4.23	0.15	2.44	0.00	1.54	0.03	0.01	0.59	0.37	0.01	0.61	0.38	0.01
	32	5	54.93	0.02	28.02	0.60	0.04	11.29	4.91	0.20	2.48	0.00	1.49	0.02	0.00	0.55	0.43	0.01	0.55	0.44	0.01
Natural B	27	5	52.85	0.05	29.23	0.87	0.15	12.56	4.16	0.13	2.40	0.00	1.57	0.03	0.01	0.61	0.37	0.01	0.62	0.37	0.01
	28	3	59.70	0.39	22.76	2.54	0.63	8.56	4.87	0.54	2.69	0.01	1.21	0.10	0.04	0.41	0.43	0.03	0.47	0.49	0.04

FeO* indicates that all iron is recalculated as ferrous iron
[a]An appropriate amount of glass has been subtracted from the plagioclase analyses (see text for details)
[b]Errors are not given for plagioclase analyses because the correction for glass contamination made it difficult to estimate quantitatively

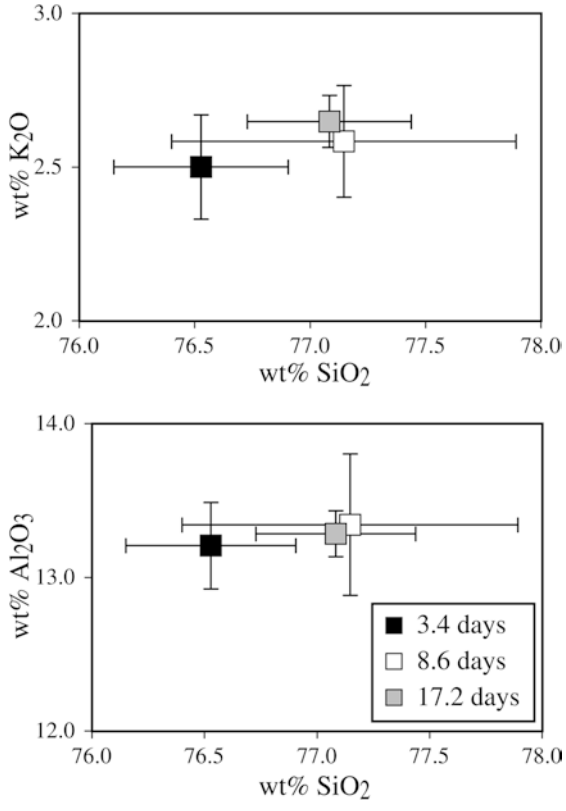

Fig. 1 Glass compositions from sample 816-4 at 1,050°C for run durations of 3.4, 8.6, and 17.2 days. The data are compiled in Table 3. One standard deviation *error bars* are shown for each point. Note the very compressed wt% SiO_2 scale and the resulting *large error bars*

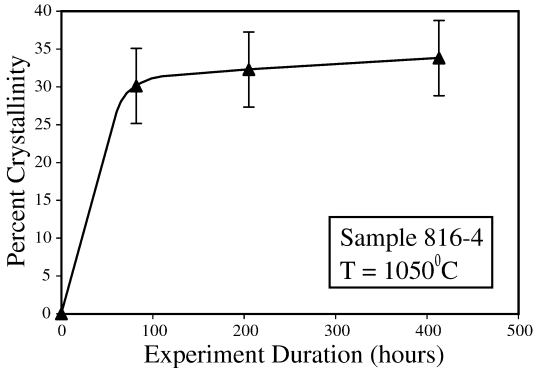

Fig. 2 Calculated crystallinity of sample 816-4 at 1,050°C as a function of experimental duration. As the duration of the experiment increases, the crystal content reaches a plateau, indicating an approach to equilibrium in experiments lasting at least 3.5 days

Phase relations

Liquidus constraints

All three initial melt compositions lack crystals at 1,250 °C but contain them at 1,200 °C, thus constraining their one-atmosphere liquidus temperature between 1,200 and 1,250 °C (that of 816-4 is further constrained to lie between 1,200 and 1,225 °C) (Table 2). A silica phase (hereafter referred to as quartz) is the liquidus phase in the most silicic sample 816-4, with plagioclase and unidentified Mg-Fe-Ti oxides crystallizing between 1,200 and 1,150 °C. Intermediate sample 722-5 has plagioclase as the liquidus phase, with quartz crystallizing by 1,150 °C, oxides by 1,100 °C, and orthopyroxene by 1,000 °C. In the most mafic sample, 816-3, plagioclase is the liquidus phase with quartz, oxides and orthopyroxene crystallizing by 1,100 °C, and clinopyroxene appearing by 1,050 °C.

Glass compositions

The ranges in glass compositions produced from all three synthetic starting materials are plotted together in Fig. 3 as a function of temperature. Potassium behaves incompatibly in all samples, increasing in concentration as the temperature decreases and crystallinity increases. Conversely, calcium displays compatible behavior, decreasing as a consequence of plagioclase crystallization. Pyroxene crystallization is best monitored by Mg abundance, which increases in the melt until pyroxene forms and then decreases.

In the most mafic sample 816-3, the silica content in the glass increased from 67.3 to approximately 76.5 wt% SiO_2 between 1,250 and 1,000 °C. In the intermediate sample 722-5, silica increased only 3.0 wt%, beginning at 73.7 wt% SiO_2 and again ending at ~76.5 wt% SiO_2. Neither sample produced glass more siliceous than this maximum. By contrast, the most silicic sample, 816-4, started with an SiO_2 content of 78.1 wt%, higher than this inferred "maximum." As the temperature of this sample decreased to 1,000 °C, the glass silica content decreased 2.2 to ~76 wt% SiO_2 as a result of quartz crystallization, indicating that the bulk composition of sample 816-4 is on the quartz side of the quartz-feldspar cotectic. With decreasing temperature, melts in all three samples evolved to a final glass silica composition of 76 ± 1 wt%, suggesting that this corresponds approximately to the silica content of the one-atmosphere quartz-feldspar cotectic.

Plagioclase compositions

The compositions of plagioclase (corrected for glass contamination as described above) formed over the temperature range 1,000 to 1,200 °C are shown in Fig. 4. Although plagioclase is present at 1,200 °C in the intermediate and most mafic samples 722-5 and 816-3, individual crystals in the intermediate sample were too small and too scarce to analyze. All plagioclase crystals

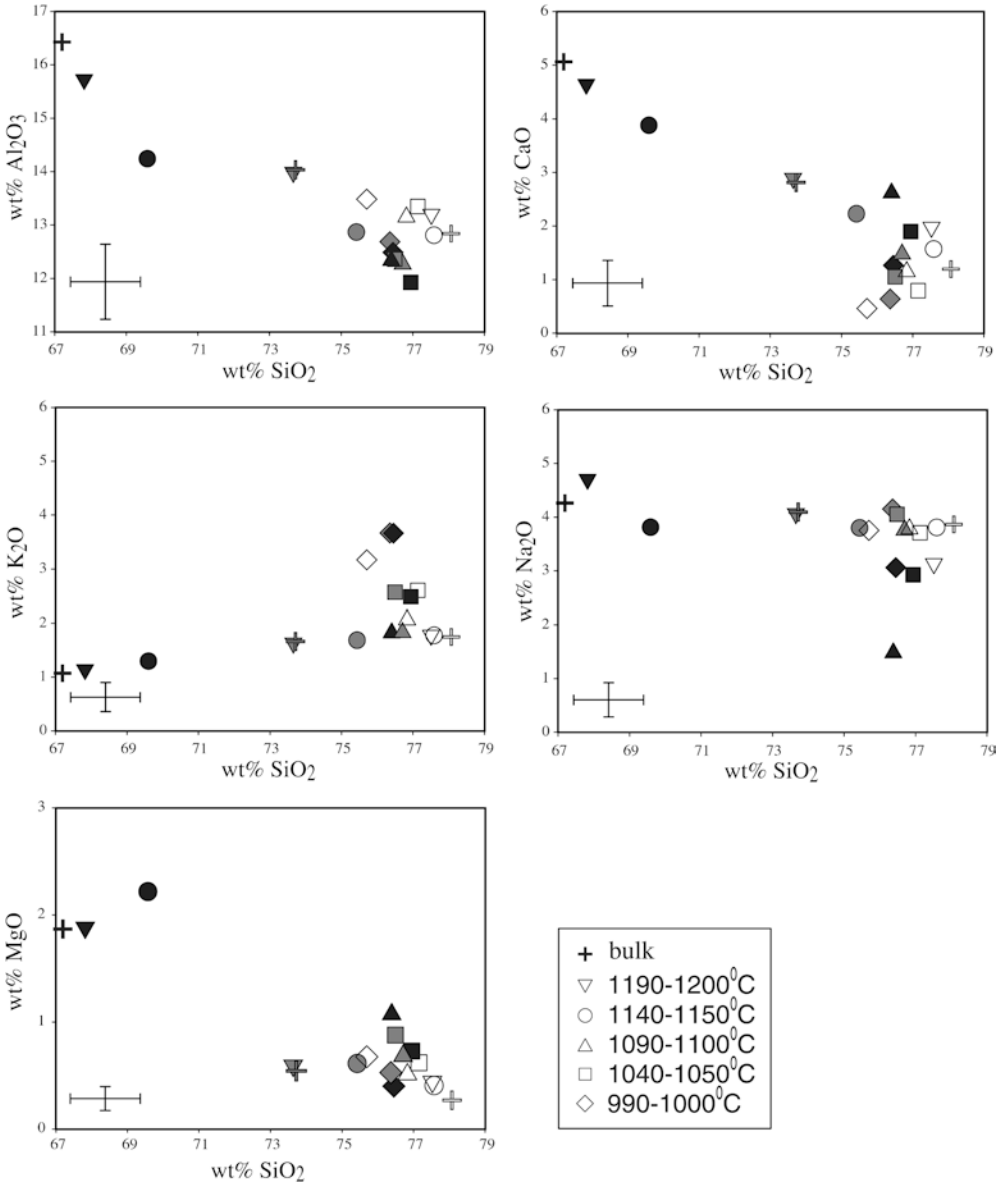

Fig. 3 Harker diagrams comparing glass compositions for each sample over the range of investigated temperatures. *Black symbols* Sample 816-3; *gray symbols* sample 722–5; *open symbols* sample 816–4. Note the vertical scale of the MgO plot is half that of the other plots. *Temperatures* are given as a range of values, for the actual temperature of each run see Table 2. *Error bars* represent the maximum one standard deviation error of any of the plotted points

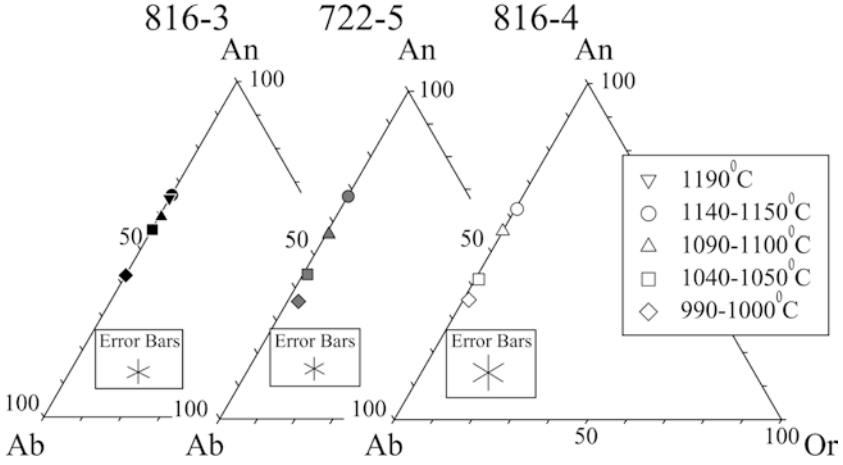

Fig. 4 Compositions of plagioclase grains in each sample over a range of temperatures plotted on anorthite-albite-orthoclase (An-Ab-Or) ternary diagrams. Sample 816-3 (*black symbols*), sample 722–5 (*gray symbols*), sample 816–4 (*open symbols*). None of the samples displayed compositional zoning. *Temperatures* are given as a range of values, for the actual temperature of each run see Table 2. *Error bars* represent the maximum one standard deviation error for all the points plotted on that diagram

plot along the An-Ab plagioclase join, with orthoclase components generally accounting for less than 1 mol%. The small Or component is anticipated as the solubility of potassium in plagioclase decreases with decreasing pressure (Nelson and Montana 1992; Fuhrman and Lindsley 1988).

All samples show a similar strong dependence of plagioclase composition on run temperature. The first plagioclase crystals to form in each sample are calcium-rich labradorites, and as the temperature decreases, the amount of calcium available in the melt decreases and plagioclase compositions shift toward sodium-rich andesine (Fig. 4 and Table 4).

Melting experiments

Natural sample A has a bulk composition reasonably similar to synthetic sample 816-3, and thus a comparison of the temperature-phase composition relations of these two sets of experiments provides a rough test of reversibility and hence equilibrium. Glass compositions vary significantly over the temperature interval investigated and those produced in the melting experiments are very similar (within 2σ error bars) to those in the crystallization experiments at the same temperatures (Fig. 5). The largest overall discrepancy between the glasses produced in the two samples is in FeO, the oxide that varies most between the two bulk compositions (Table 3). The close match of glass compositions from melting and crystallization experiments indicates

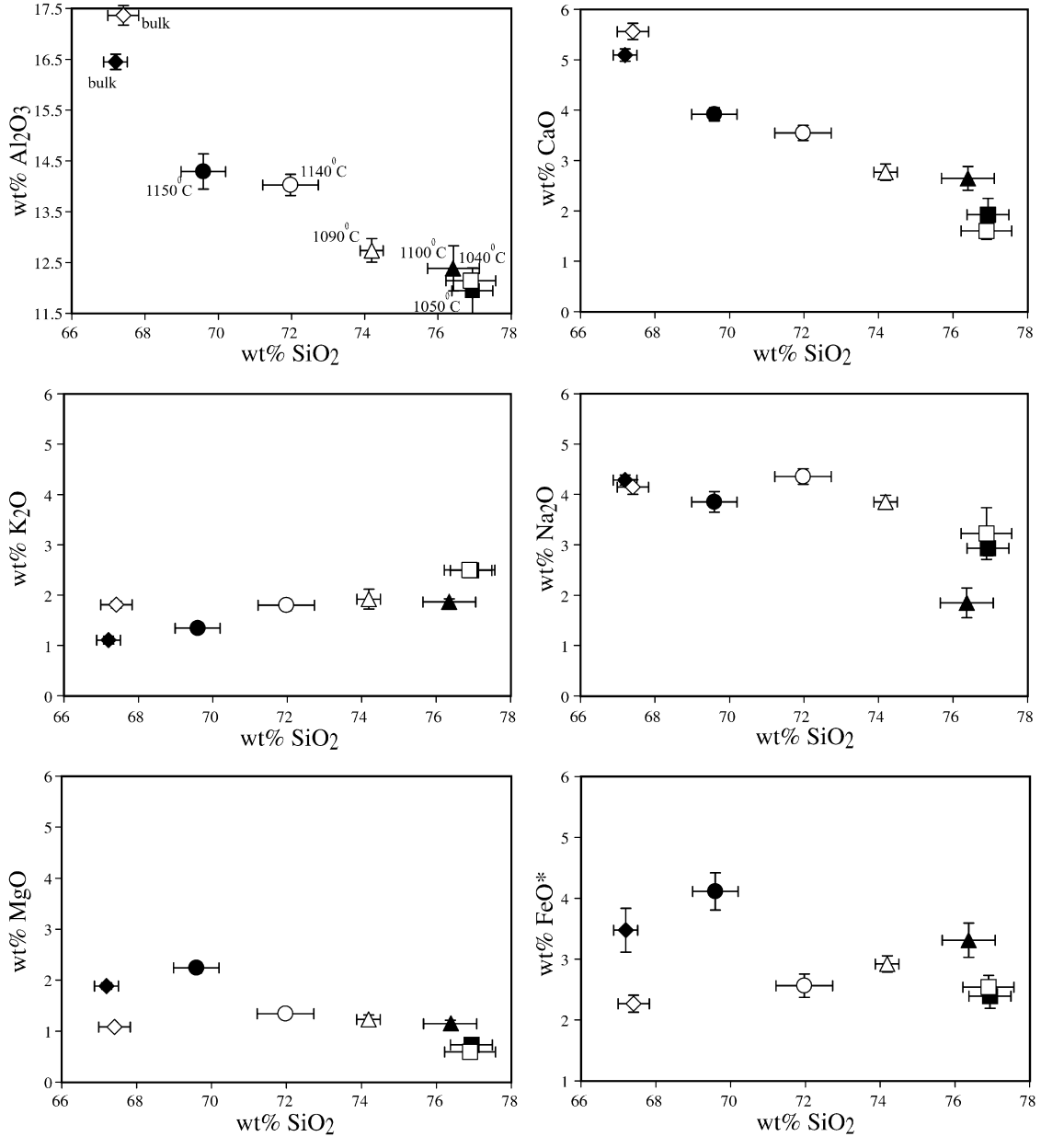

Fig. 5 Harker diagrams comparing glass compositions in crystallization experiments on sample 816-3 (*filled symbols*) and melting experiments on natural sample A (*open symbols*). While the bulk compositions of these two samples are similar (*diamonds*), they are not exactly the same. Thus at any given temperature the two samples are not expected to have exactly the same compositions. The temperatures given in the first diagram apply to every plot. *Error bars* represent one standard deviation. Where the vertical error bars are not visible, they are smaller than the symbol

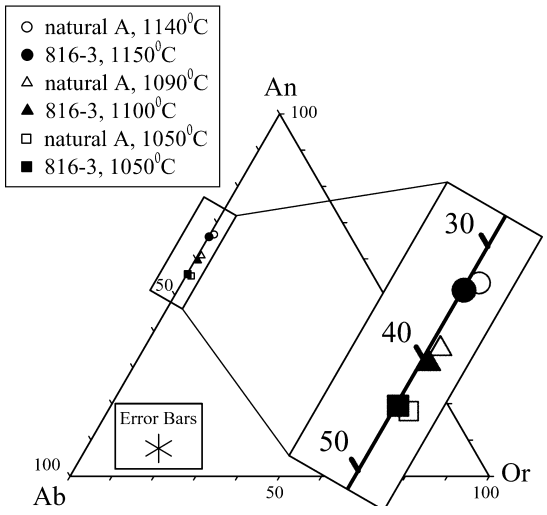

Fig. 6 Compositions of plagioclase crystals from crystallization experiments on sample 816-3 (*filled symbols*) and melting experiments on natural sample A (*open symbols*) plotted on an anorthite-albite-orthoclase (An-Ab-Or) ternary diagram. *Error bars* represent the maximum one standard deviation error. At each temperature, the plagioclase crystals from crystallization and melting experiments have the same compositions, within error

that compositional equilibrium was closely approached in both sets of experiments. The similarity of plagioclase compositions in the melting and crystallization experiments further supports this interpretation (Fig. 6). Also, we note that the phase assemblages produced at each run temperature were the same in the two types of experiments (compare 816-3 and natural A in Table 2), despite their small differences in bulk composition.

Discussion

Attainment of equilibrium

Low-pressure phase relations in synthetic silicic systems are poorly defined because of the difficulty in reaching equilibrium on laboratory time-scales in these viscous melts (e.g., Schairer 1950). However, all previous studies of such systems at one-atmosphere have focused on simple, and refractory, two-, three-, or four-component synthetic systems (e.g., Qz-Ab, Qz-Ab-Or), rather than natural multi-component systems (Bowen 1913; Schairer 1950; Tuttle and Bowen 1958; Tsuchiyama and Takahashi 1983; Johannes et al. 1994). The small amount of network modifiers, such as magnesium and iron, present in natural melts significantly reduces their viscosities, increases diffusivities, and increases reaction rates (Johannes et al. 1994; Baker 1995). For the melts of this study, calculated viscosities (e.g., Shaw 1972) increase by an order of magnitude when the Fe, Mg, and Ti are numerically removed. As a result, in this study of natural multi-component silicic melts, equilibrium was closely approached on time scales ≥3.5 days, even for our most silicic composition at relatively low temperature (1,050 °C).

Significance of bulk composition

The samples examined in this study range in bulk SiO_2 content from 67.2 to 78.1 wt%, yet they all have liquidus temperatures between 1,200 and 1,250 °C. This is consistent with dry liquidus temperatures of >1,200 °C determined by Whitney (1975) at 200 MPa for various compositions in the system Qz-Ab-Or-An. Liquidus temperatures increase dramatically as H_2O contents decrease, although on most phase diagrams liquidus curves are dashed as they approach one-atmosphere due to lack of data at these conditions (e.g., Johannes and Holtz 1996). Liquidus temperatures as high as those documented here suggest that one-atmosphere anhydrous silicic liquidus temperatures are higher than previously estimated, in fact they are nearly equivalent to the liquidus temperatures found in more mafic systems (Grove et al. 1982). As suggested by Becker et al. (1998) and Holtz et al. (2001), dry silicic liquidus temperatures given in the literature (Huang and Wyllie 1975; Ebadi and Johannes 1991) are probably underestimated because the quartz and feldspar starting materials contain small amounts of water, which leads to the formation of melt at lower temperatures.

The relative effects of temperature and silica content on the crystallization temperature of each phase are shown in Fig. 7, a summary of our results. We believe that these samples can be reasonably linked in a diagram of this type since they all erupted from the same volcanic center and likely represent derivatives of one another. Steeply dipping mineral-in boundaries in Fig. 7 indicate strong compositional control, while shallow dipping boundaries indicate that the temperature of phase appearance is nearly independent of composition. Our data do not constrain the slope of the plagioclase-in curve very well, but we suggest a low angle, consistent with data of Grove et al. (1982) showing that plagioclase is on the one-atmosphere liquidus of more mafic compositions (e.g., 54.5 wt% SiO_2) near 1,200 °C. The near-horizontal orientation of the plagioclase phase boundary suggests that its crystallization is more dependent on temperature than the bulk silica content of the sample. Oxides also appear little affected by bulk composition, although their temperature of appearance decreases slightly with decreasing bulk silica. This behavior may reflect the nearly constant oxygen fugacity in the experiments. In contrast, the appearance of quartz shows a strong compositional control. Quartz is both more abundant and crystallizes earlier in high-silica melts than in melts with lower silica contents. The appearance of orthopyroxene and clinopyroxene is controlled by both temperature and bulk composition, with a strong temperature control in more mafic compositions and an upper compositional limit at silica contents of ~75 wt%.

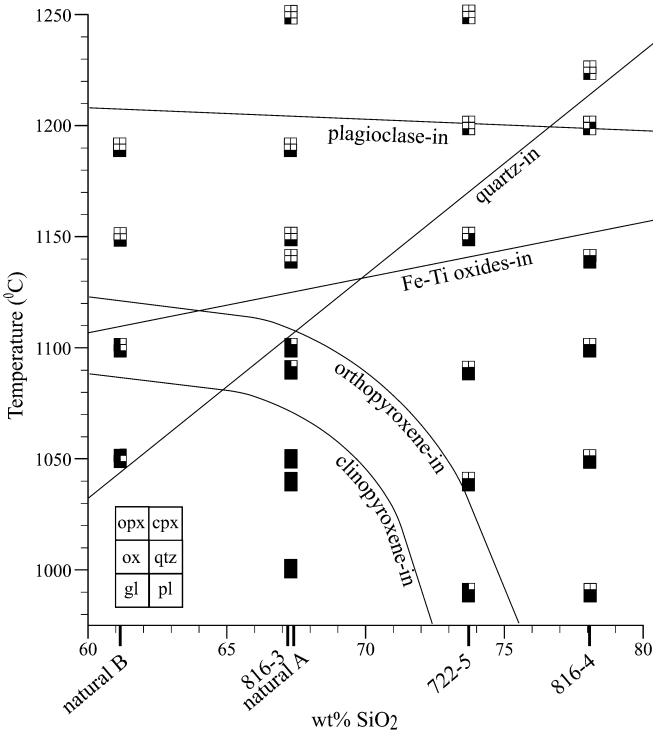

Fig. 7 Summary phase diagram of temperature versus bulk silica content in each sample. Due to their similar bulk compositions, results for sample 816-3 and natural A were combined. The plagioclase box for sample 722-5 at 1,200°C is shaded *gray* because this sample contains only a few, very small plagioclase crystals, and is therefore very close to the plagioclase-in temperature. The *plagioclase-in curve* was drawn near horizontal based on the plagioclase-in temperatures found by Grove et al. (1982) for more mafic compositions

Qz-Ab-Or diagram

The haplogranite system quartz-albite-orthoclase (Qz-Ab-Or) provides a useful means of comparing silicic melt compositions. Phase relations in the Qz-Ab-Or system are well defined for pressures between 50 and 500 MPa and water-saturated conditions (Tuttle and Bowen 1958; Luth et al. 1964; Ebadi and Johannes 1991; Holtz et al. 1992a). At pressures below 500 MPa there are two primary phase volumes, quartz and feldspar, separated by a curved cotectic (Fig. 8). The square on each cotectic is the thermal minimum, and represents the final composition of a crystallizing melt at any given pressure. There are no reliable experimental data on the Qz-Ab-Or ternary at pressures below 50 MPa because of difficulties in reach-

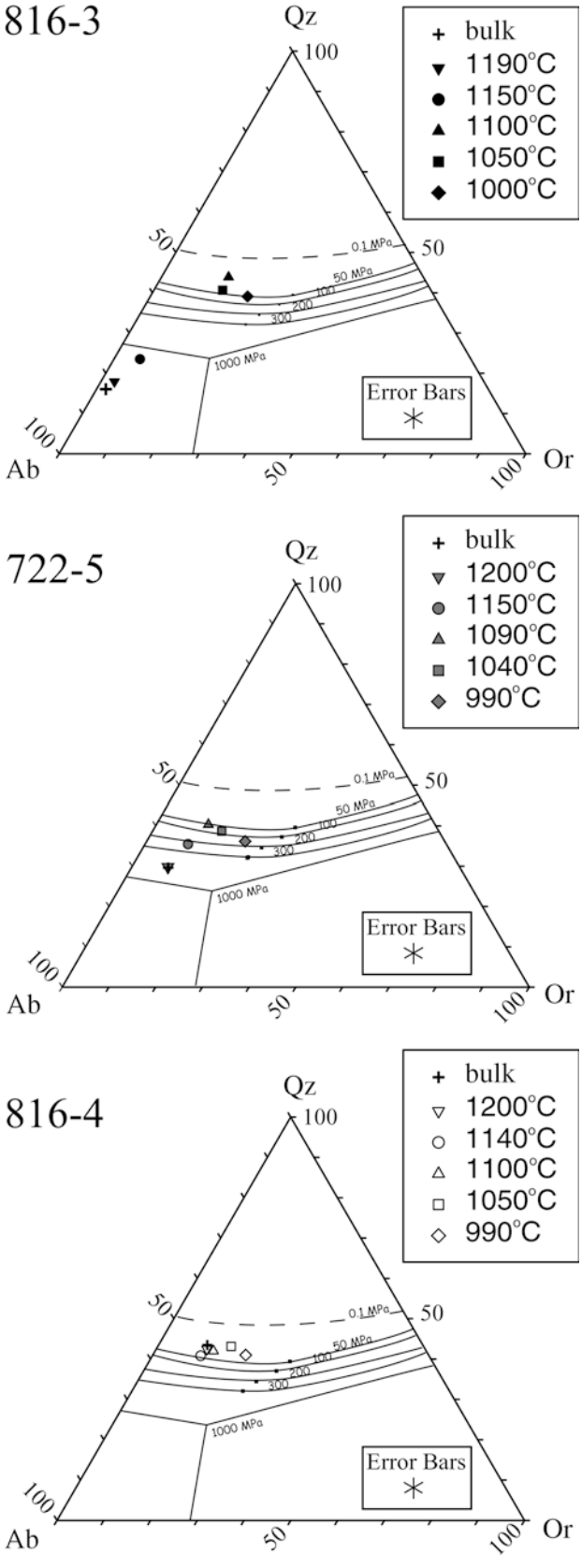

Fig. 8 Projection of glass compositions in experimental runs into the Qz-Ab-Or system using the projection scheme of Blundy and Cashman (2001). Sample 816-3 (*black symbols*), sample 722–5 (*gray symbols*), sample 816-4 (*open symbols*). The correction does not account for the effect of normative corundum. Due to corundum >1%, all 816-4 samples should move down slightly (~3 wt% away from Qz apex) and the 816-3 sample at 1,100°C with quartz should move down ~4 wt%. Correcting for normative corundum will bring these samples more in-line with the other experiments. Previous estimates of the 300, 200, 100, 50, and 0.1 MPa (1 atm) water-saturated quartz-feldspar cotectics and minima (*squares*) are shown. Data from Tuttle and Bowen (1958), Luth et al. (1964), Ebadi and Johannes (1991)

ing equilibrium (Schairer 1950), therefore the one-atmosphere (0.1 MPa) cotectic is dashed in Fig. 8, approximated by Blundy and Cashman (2001) from the experiments of Schairer (1950). During isobaric cooling, melts evolve toward the appropriate pressure cotectic, and then down the cotectic toward the thermal minimum.

Glass compositions from the multi-component silicic samples used in these experiments were projected into the Qz-Ab-Or system using the empirical projection scheme of Blundy and Cashman (2001) (Fig. 8), which corrects for small amounts (< 20%) of normative anorthite. In their Fig. 3 these authors showed that this projection scheme shifts the positions of experimental melts like ours, saturated in quartz and plagioclase, to new positions in the Qz-Ab-Or diagram on or near the appropriate quartz-feldspar cotectics for the pressure of the experiments. For each point in Fig. 8, the plotted components, Qz, Ab, and Or, account for a substantial majority (average of ~82%) of the normative description of the melt. While this projection does correct for normative anorthite, it does not account for the effect of normative corundum, which is greater than 1% in sample 816-3 at 1,100 °C (2.9%) and all glasses from sample 816-4 (1.8–3.1%). Excess alumina shifts points toward more Qz-rich compositions (Holtz et al. 1992c; Johannes and Holtz 1996), thus a correction for the normative corundum in these samples would reduce Qz by ~2 wt% for melts with ~2.5 wt% normative corundum (Blundy and Cashman 2001), bringing these samples more in-line with the others.

Samples 816-3 and 722-5 have initial melt (bulk) compositions well within the feldspar stability field in the Qz-Ab-Or diagram (Fig. 8). Thus, plagioclase is the first phase to crystallize in these samples. As plagioclase crystallizes, it drives the composition of the melt away from albite toward the quartz-feldspar cotectic and more silicic compositions. By 1,100 °C these samples have begun crystallizing quartz and their glass compositions have theoretically reached the one-atmosphere quartz-feldspar cotectic. Co-crystallization of plagioclase and quartz then drives the glass compositions along the quartz-feldspar cotectic to the right, toward the thermal minimum.

The bulk initial melt composition of sample 816-4 also plots within the feldspar stability field based on the one-atmosphere cotectic estimated by Blundy and Cashman (2001) (Fig. 8). However, the first phase to crystallize in this sample is quartz (by 1,200 °C) which drives the composition of the melt to less silicic compositions and by 1,140 °C plagioclase begins crystallizing. The difference in glass compositions between the 1,200 and 1,140 °C runs is very small, suggesting that the bulk composition of this sample lies very close to the true quartz-feldspar one-atmosphere cotectic.

In all samples at 1,000–1,100 °C, quartz and plagioclase display intergrowth textures suggestive of cotectic crystallization (e.g. Fig. 9). However, the normative quartz contents in each of these melts fall significantly short of the one-atmosphere cotectic previously estimated by Blundy and Cashman (2001), who noted the large uncertainty in the data of Schairer (1950), upon which their placement of the cotectic was based. Accordingly, we have revised the estimated location of this phase boundary, moving it away from quartz to a position consistent with our experimental observations (Fig. 10). We stress that our low temperature run products do not contain alkali feldspar and thus we cannot claim to have truly located the one-atmosphere quartz-alkali feldspar cotectic in the Qz-Ab-Or diagram. However, judging from the success of Blundy and Cashman (2001) in projecting experimental quartz- and plagioclase-saturated melts like ours onto the appropriate pressure cotectics in the Qz-Ab-Or system, we believe that our revised one-atmosphere cotectic is appropriately placed (Fig. 10). We also note that our lower temperature glasses, which we use to define the position of this cotectic, consist predominantly (83–92 mol%) of normative Qz + Ab + Or and thus little distortion is expected to result from this projection. Our proposed location of the one-atmosphere cotectic also seems in line with extrapolation of the higher-pressure cotectics to one-atmosphere (Fig. 10).

The melt phase in all three of our bulk compositions reaches the new one-atmosphere cotectic by 1,100 °C, in agreement with the quartz and plagioclase co-crystallization textures observed in each sample at this, and lower temperatures. Additionally, along the cotectic, all three samples plot in the same general location within error, and help to define the thermal gradient along the cotectic as the minimum is approached (Fig. 10).

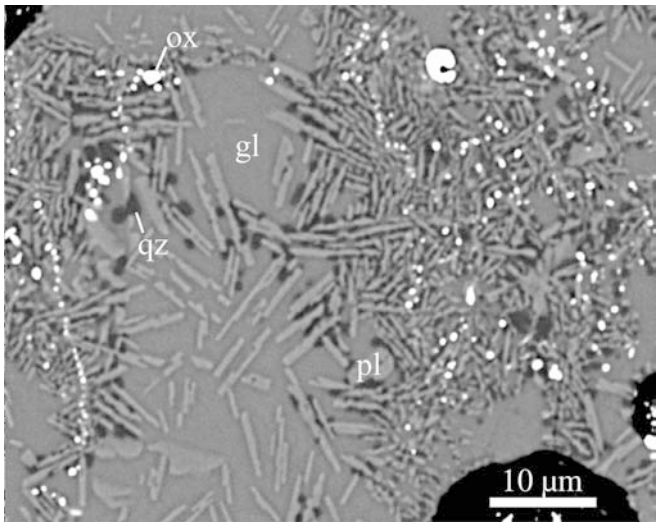

Fig. 9 BSE image of quartz-plagioclase co-crystallization texture in sample 722-5 at 1,050°C. This texture is found in each sample between 1,000 and 1,100°C, consistent with the temperature interval over which these samples plot along the quartz-feldspar cotectic in the Qz-Ab-Or system. This patchy texture is not merely an experimental phenomenon, but is also found in volcanic deposits where the magma stalled and crystallized at shallow depths and in domes and spines (Cashman and Blundy 2000). Examples of each phase are labeled. The *black areas* are holes or blemishes in the surface of the sample

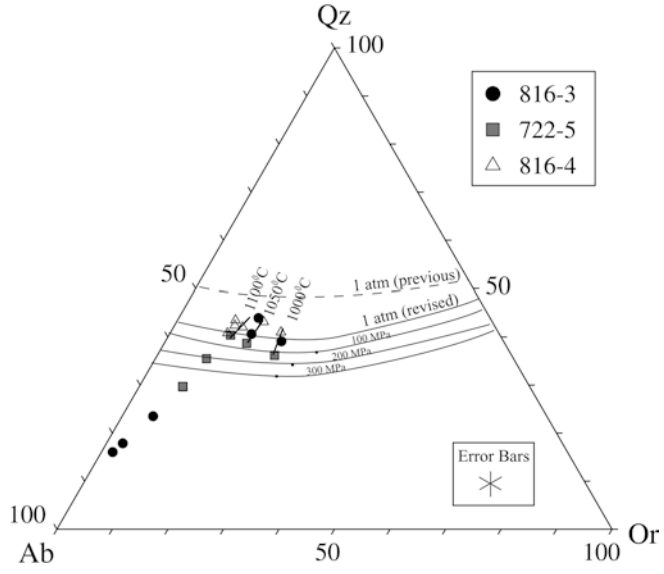

Fig. 10 Qz-Ab-Or projection of experimental samples 816–3, 722–5, and 816–4 from 1,250 to 1,000°C (for the temperature of each symbol see Fig. 10). Between 1,100 and 1,000°C these samples define a new one-atmosphere quartz-feldspar cotectic, which is further from the Qz-apex than previously estimated (Tuttle and Bowen 1958). Isotherms along the cotectic are defined by the clustering of experiments at each temperature

Significance of quartz crystallization

Groundmass quartz is found in silicic volcanic rocks only when magma has stalled in the conduit or when it ascends slowly (Hammer et al. 1999; Cashman and Blundy 2000; Blundy and Cashman 2001). This suggests that low-pressure quartz nucleation may be kinetically inhibited, with nucleation requiring a lag time, probably because of its highly polymerized structure. In decompression experiments, melts that experienced high degrees of effective undercooling (~200 °C) were found to suppress quartz formation in runs as long as 168 hours (Hammer and Rutherford 2002). However, in the isothermal one-atmosphere experiments of this study, quartz crystallized at an undercooling of 200 °C in runs of only 74 h (shortest duration examined at this degree of undercooling), and at an undercooling of ~100 °C in runs as short as 24 h (the shortest duration examined in this study). Therefore, rates of quartz nucleation and growth appear to depend on the rate of decompression, the degree of undercooling, the pressure, and the magma cooling rate (the amount of time it has to equilibrate). The absence of quartz in eruptive deposits suggests that these magmas either cooled quickly, or they decompressed rapidly and thus experienced a high degree of undercooling. Alternatively, water in natural samples may inhibit quartz nucleation by depolymerizing the melt. In any case, the absence of quartz in natural samples indicates that their magmas did not equilibrate with surface conditions.

Summary and implications

The matrix glass in every experimental sample evolved to 76 ± 1 wt% SiO_2, regardless of its initial bulk composition (Fig. 3). Similarly, the final melt (glass) compositions found in the 1986 eruption deposits of Augustine Volcano fall within the narrow range of silica contents (75.2 and 78.2 wt%), even though their initial melt compositions (i.e. groundmasses) ranged from 65.0 to 77.2 wt% SiO_2 and their bulk compositions ranged from 58.5 to 63.2 (Roman 2001). The similar evolution of silica contents in glasses derived from initially quite different bulk compositions suggests that this is the approximate silica content of the one-atmosphere cotectic. Regardless of the initial melt compositions, crystallization of various phases in different proportions drives them toward similar final compositions, where subsequent crystallization will hold the composition of the melt steady. Therefore, ~76–77 wt% SiO_2 may represent an upper limit to attainable silica contents in magmas such as these.

Glasses with silica contents greater than ~76–77 wt% SiO_2 are common in some eruptive deposits (Cashman and Blundy 2000; Roman 2001; Blundy and Cashman 2001; Hammer et al. 1999; Wolf and Eichelberger 1997). Our experiments suggest that these high silica glasses result from magmas that overshot the quartz-feldspar cotectic during ascent. When magma is highly undercooled it will crystallize rapidly in an effort to attain equilibrium. Due to kinetic delays associated with nucleation and growth of quartz, rapidly undercooled magmas may continue to crystallize only plagioclase, even after they reach the quartz-feldspar cotectic. This would drive the glass composition past the quartz-feldspar cotectic into the quartz stability field, resulting in higher silica contents than expected at equilibrium. This interpretation is supported by new experimental data of Martel and Schmidt (2003) who found that plagioclase crystallized readily in their decompression experiments, but silica contents reached 80 wt% prior to the onset of cristobalite crystallization. In summary, anomalously high silica contents provide evidence of non-equilibrium crystallization resulting from high degrees of effective undercooling (250–300 °C, based on the high liquidus temperatures of our experiments) created during decompression and volatile exsolution, and kinetic barriers to nucleation and growth of a silica phase.

Acknowledgements We would like to thank Michael Shaffer for his assistance with electron microprobe analyses and SEM imaging. This work was supported by NSF grant EAR-9909509 to K.V.C. and A.D.J. The electron microbeam facility of the University of Oregon was acquired with NSF grant EAR-8803960 with a matching grant from the Keck Foundation, and technician support was provided by NSF grant EAR-9712115. We are also grateful for two thorough anonymous reviewers.

References

Baker DR (1995) Diffusion of silicon and gallium (as an analogue for aluminum) network-forming cations and their relationship to viscosity in albite melt. Geochim Cosmochim Acta 59(17):3561–3571

Bartels G (1987) Das Schmelzen von Plagioklas im System Qz-Ab-An-H_2O. Diplomarbeit, Universität Hannover

Becker A, Holtz F, Johannes W (1998) Liquidus temperatures and phase compositions in the system Qz-Ab-Or at 5 kbar and very low water activities. Contrib Mineral Petrol 130:213–224

Blundy JD, Cashman KV (2001) Ascent-driven crystallisation of dacite magmas at Mount St. Helens, 1980–1986. Contrib Mineral Petrol 140:631–650

Boettcher AL, Guo Q, Bohlen SR, Hanson B (1984) Melting in feldspar-bearing systems to high pressures and the structure of aluminosilicate liquids. Geology 12:202–204

Bohlen SR, Boettcher AL, Wall VJ, Clemens JD (1983) Stability of phlogopite-quartz and sanidine-quartz: a model for melting in the lower crust. Contrib Mineral Petrol 83:270–277

Bowen NL (1913) The melting phenomena of the plagioclase feldspars. Am J Sci 35:577–599

Brugger (2001) Experimental determination of one-atmosphere phase relations for melt compositions of Augustine Volcano. MS Thesis, Department of Geological Sciences, University of Oregon, 145 pp

Cashman KV (1992) Groundmass crystallization of Mount St. Helens dacite, 1980–1986: A tool for interpreting shallow magmatic processes. Contrib Mineral Petrol 109:431–449

Cashman KV, Blundy JD (2000) Degassing and crystallization of ascending andesite and dacite. Philos Trans R Soc Lond 358:1487–1513

Clemens JD, Wall VJ (1981) Origin and crystallization of some peraluminous (S-type) granitic magmas. Can Mineral 19:111–131

Clemens JD, Holloway JR, White AJR (1986) Origin of an A-type granite: experimental constraints. Am Mineral 71:317–324

Conrad WK, Nicholls IA, Wall VJ (1988) Water-saturated and – undersaturated melting of metaluminous and peraluminous crustal compositions at 10 kb: evidence for the origin of silicic magmas in the Taupo Volcanic Zone, New Zealand, and other occurrences. J Petrol 29:765–803

Dimitriadis S (1978) Some liquid compositions in the peraluminous haplo-granite system. Neues Jahrb Miner Monatsh 1978:377–383

Ebadi A, Johannes W (1991) Beginning of melting and composition of first melts in the system Qz-Ab-Or-H_2O-CO_2. Contrib Mineral Petrol 106:286–295

Fuhrman ML, Lindsley DH (1988) Ternary-feldspar modeling and thermometry. Am Mineral 73:201–215

Gardner CA, Cashman KV, Neal CA (1998) Tephra-fall deposits from the 1992 eruption of Crater Peak, Alaska: implications of clast textures from eruptive processes. Bull Volcanol 59:537–555

Grove TL, Gerlach DC, Sando TW (1982) Origin of calc-alkaline series lavas at Medicine Lake Volcano by fractionation, assimilation and mixing. Contrib Mineral Petrol 80:160–182

Hammer JE, Rutherford MJ (2002) An experimental study of the kinetics of decompression-induced crystallization in silicic melt. J Geophys Res 107

Hammer JE, Cashman KV, Voight B (2000) Magmatic processes revealed by textural and compositional trends in Merapi dome lavas. J Volcanol Geotherm Res 100:165–192

Hammer JE, Cashman KV, Hoblitt RP, Newman S (1999) Degasing and microlite crystallization during pre-climactic events of the 1991 eruption of Mt. Pinatubo, Phillipines. Bull Volcanol 60:355–380

Huebner JS, Sato M (1970) The oxygen fugacity-temperature relationships of manganese oxide and nickel oxide buffers. Am Mineral 55:934–952

Holtz F, Johannes W (1991) Genesis of peraluminous granites I. Experimental investigation of melt compositions at 3 and 5 kb and various H_2O-activities. J Petrol 32:935–958

Holtz F, Pichavant M, Barbey P, Johannes W (1992a) Effects of H_2O on the liquidus phase relations in the haplogranite system at 2 and 5 kbar. Am Mineral 77:1223–1241

Holtz F, Johannes W, Pichavant M (1992b) Effect of excess aluminum on phase relations in the system Qz-Ab-Or. Experimental investigation at 2 kbar and reduced H_2O-activity. Eur J Mineral 4:137–152

Holtz F, Johannes W, Pichavant M (1992c) Peraluminous granites; the effect of alumina on melt composition and coexisting minerals. Proc 2nd Hutton Symposium on the Origin of granites and related rocks, 272, pp 409–416

Holtz F, Becker A, Freise M, Johannes W (2001) The water-undersaturated and dry Qz-Ab-Or system revisited. Experimental results at very low water activities and geological implications. Contrib Mineral Petrol 141:347–357

Huang WL, Wyllie PJ (1975) Melting reactions in the system Na-$AlSi_3O_8$-$KAlSi_3O_8$-H_2O to 35 kilobars, dry and with excess water. J Geol 83:737–748

Huang WL, Wyllie PJ (1981) Phase relations of S-type granite with H2O to 35 kbar as a model for fusion of metamorphosed subducted oceanic sediments. Contrib Mineral Petrol 42:1–14

James RS, Hamilton DL (1969) Phase relations in the system $NaAlSi_3O_8$-$KAlSi_3O_8$-$CaAlSi_3O_8$ at 1 kilobar water vapour pressure. Contrib Mineral Petrol 21:111–141

Johannes W (1978) Melting of plagioclase in the system Ab-An-H_2O and Qz-Ab-An-H_2O at $P_{H2O} = 5$ kbars, an equilibrium problem. Contrib Mineral Petrol 66:295–303

Johannes W (1984) Beginning of melting in the granite system Qz-Ab-Or-An-H_2O. Contrib Mineral Petrol 84:264–273

Johannes W (1989) Melting of plagioclase-quartz assemblages at 2 kbar water pressure. Contrib Mineral Petrol 103:270–276

Johannes W, Holtz F (1996) Petrogenesis and experimental petrology of granitic rocks. Springer, Berlin Heidelberg New York, 335 pp

Johannes W, Koepke J, Behrens H (1994) Partial melting reactions of plagioclase and plagioclase-bearing systems. In: Parsons I (ed) Feldspars and their reactions, NATO ASI Series, vol 421. Kluwer, London, pp 161–194

Johnson MC, Rutherford MJ (1989) Experimentally determined conditions in the Fish Canyon Tuff, Colorado, magma chamber. J Petrol 30:711–737

Joyce DB, Voigt DE (1994) A phase equilibrium study in the system $KAlSi_3O_8$-$NaAlSi_3O_8$-SiO_2-Al_2SiO_5-H_2O and petrogenetic interpretations. Am Mineral 79:504–512

Lambert IB, Robertson JK, Wyllie PJ (1969) Melting reactions in the system $KAlSi_3O_8$-SiO_2-H_2O to 18.5 kilobars. Am J Sci 267:609–626

Le Breton N, Thompson AB (1988) Fluid-absent (dehydration) melting of biotite in metapelites in the early stages of anatexis. Contrib Mineral Petrol 99:226–237

Luth WC (1969) The systems $NaAlSi_3O_8$-SiO_2 and $KAlSi_3O_8$-SiO_2 to 20 kb and the relationship between H_2O-content, P_{H2O}, and P_{total} in granitic magmas. Am J Sci A-267:325–341

Luth WC, Jahns RH, Tuttle OF (1964) The granite system at pressures of 4 to 10 kilobars. J Geophys Res 69:759–773

Martel C, Schmidt B (2003) Decompression experiments as an insight into ascent rates of silicic magmas. Contrib Mineral Petrol 144:397–415

Melnik O, Sparks R (1999) Nonlinear dynamics of lava dome extrusion. Nature 402:37–41

Merrill RB, Robertson JK, Wyllie PJ (1970) Melting reactions in the system $NaAlSi_3O_8$-$KAlSi_3O_8$-SiO_2-H_2O to 20 kilobars compared with results for other feldspar-quartz-H_2O and rock-H_2O systems. J Geol 82:589–606

Morgan GB, London D (1996) Optimizing the electron microprobe analysis of hydrous alkali aluminosilicate glasses. Am Mineral 81:1176–1185

Muncill GE, Lasaga AC (1987) Crystal-growth kinetics of plagioclase in igneous systems: one-atmosphere experiments and application of a simplified growth model. Am Mineral 72:299–311

Naney MT (1983) Phase equilibria of rock-forming ferromagnesian silicates in granitic systems. Am J Sci 283:993–1033

Nelson ST, Montana A (1992) Sieve-textured plagioclase in volcanic rocks produced by rapid decompression. Am Mineral 77:1242–1249

Nielsen CH, Sigurdsson H (1981) Quantitative methods for electron microprobe analysis of sodium in natural and synthetic glasses. Am Mineral 66:547–552

Pichavant M, Holtz F, McMillan P (1992) Phase relations and compositional dependence of H_2O solubility in quartz-feldspar melts. Chem Geol 96:303–319

Pouchou JL, Pichoir F (1991) Quantitative analysis of homogeneous or stratified microvolumes applying the model "PAP". In: Heinrich K, Newbury D (eds) Electron probe quantitation. Plenum Press, London, pp 31–75

Puziewicz J, Johannes W (1988) Phase equilibria and compositions of Fe-Mg-Al-minerals and melts in water-saturated peraluminous granitic systems. Contrib Mineral Petrol 100:156–168

Roman D (2001) The 1986 eruption of Augustine Volcano, Alaska: magma storage and ascent. MS Thesis, Department of Geological Sciences, University of Oregon, 128 pp

Rutherford MJ, Devine JD (1988) The May 18, 1980, eruption of Mount St. Helens 3. Stability and chemistry of amphibole in the magma chamber. J Geophys Res 93:11949–11959

Rutherford MJ, Sigurdsson H, Carey M, Davis A (1985) Eruption of Mount St. Helens 1. Melt composition and experimental phase equilibria. J Geophys Res 90:2929–2947

Scaillet B, Pichavant M, Roux J (1995) Experimental crystallization of leucogranite magmas. J Petrol 36:663–705

Schairer JF (1950) The alkali-feldspar join in the system $NaAlSiO_4$-$KAlSiO_4$-SiO_2. J Geol 58:512–517

Schairer JF, Bowen NM (1935) Preliminary report on equilibrium-relations between feldspathoids, alkali feldspars and silica. Am Geophys Union Trans, 16th Annu Meet, pp 325–328

Schairer JF, Bowen NL (1955) The system K_2O-Al_2O_3-SiO_2. Am J Sci 253:681–746

Schairer JF, Bowen NL (1956) The system Na_2O-Al_2O_3-SiO_2. Am J Sci 254:129–195

Shaw HR (1963) The four-phase curve sanidine-quartz-liquid-gas between 500 and 4,000 bars. Am Mineral 48:883–896

Shaw HR (1972) Viscosities of magmatic silicate liquids: an empirical method of prediction. Am J Sci 272:870–893

Sparks RSJ (1997) Causes and consequences of pressurization in lava dome eruptions. Earth Planet Sci Lett 150:177–189

Steiner JC (1970) An experimental study of the assemblage alkali feldspar + liquid + quartz in the system $NaAlSiO_4$-$KAlSiO_4$-SiO_2-H_2O at 4,000 bars. PhD Thesis, Department of Geology, Stanford University

Steiner JC, Jahns RH, Luth WC (1975) Crystallization of alkali feldspar and quartz in the haplogranite system $NaAlSiO_4$-$KAlSiO_4$-SiO_2-H_2O at 4 kb. Geol Soc Am Bull 86:83–98

Tsuchiyama A, Takahashi E (1983) Melting kinetics of plagioclase feldspar. Contrib Mineral Petrol 84:345–354

Tuttle OF, Bowen NL (1958) origin of granite in light of experimental studies in the system NaAlSi3O8-$KalSi_3O_8$-SiO_2-H_2O. Geol Soc Am Mem 74, 153 pp

Vielzeuf D, Holloway JR (1988) Experimental determination of the fluid-absent melting relations in the pelitic system. Consequences for crustal differentiation. Contrib Mineral Petrol 98:257–276

Voight B, Sparks RSJ, Miller AD, and others (1999) Magma flow instability and cyclic activity at Soufriere Hills Volcano, Montserrat, British West Indies. Science 283:1138–1142

Voight DE, Burnham CW (1983) The solubility of Al_2SiO_5 in the system $KAlSi_3O_8$-SiO_2-H_2O at 2 kbar, and its implication for melt speciation. Trans Am Geophys Union 64:342

Whitney JA (1975) The effects of pressure, temperature, and XH_2O on phase assemblage in four synthetic rock compositions. J Geol 83:1–31

Winkler HGF, Ghose NC (1973) Further data on the eutectics in the system Qz-Or-An-H_2O. Neues Jahrb Mineral Monatsh:481–484

Winkler HGF, Boese M, Marcopoulos T (1975) Low temperature granitic melts. Neues Jahrb Mineral Monatsh;245–268

Winkler HGF, Das BK, Bretibart R (1977) Further data of low-temperature melts existing on the quartz + plagioclase + liquid + vapour isobaric cotectic surface within the system Qz-Ab-Or-An-H2O. Neues Jahrb Mineral Monatsh:241–247

Wolf KJ, Eichelberger JC (1997) Syneruptive mixing, degassing and crystallization at Redoubt Volcano, eruption of December 1989 to May 1990. J Volcanol Geotherm Res 75:19–37

Yoder HS (1968) Albite-anorthite-quartz-water at 5 kbar. Carnegie Inst Wash Yearb 66:477–478